Langmuir

Article

pubs.acs.org/Langmuir

On the Motion of Carbon Nanotube Clusters near Optical Fiber Tips: Thermophoresis, Radiative Pressure, and Convection Effects

J. Rodrigo Vélez-Cordero*[,†,§] and J. Hernández-Cordero[‡]

[†]Instituto de Física, Universidad Autónoma de San Luis Potosí, Alvaro Obregón 64, 78000 San Luis Potosí, S.L.P., México

[‡]Instituto de Investigaciones en Materiales, Universidad Nacional Autónoma de México, Apdo. Postal 70-360, México D.F. 04510, México

[§]Cátedras CONACyT, Dirección Adjunta de Desarrollo Científico del CONACyT, Av. Insurgentes Sur 1582, México D.F. 03940, México

Supporting Information

ABSTRACT: We analyze the motion of multiwalled carbon nanotubes clusters in water or ethanol upon irradiation with a 975 and 1550 nm laser beam guided by an optical fiber. Upon measuring the velocities of the nanotube clusters in and out of the laser beam cone, we were able to identify thermophoresis, convection and radiation pressure as the main driving forces that determine the equilibrium position of the dispersion at low optical powers: while thermophoresis and convection pull the clusters toward the laser beam axis (negative Soret coefficient), radiation pressure pushes the clusters away from the fiber tip. A theoretical solution for the thermophoretic velocity, which considers interfacial motion and a repulsive potential interaction between the nanotubes and the solvent (hydrophobic interaction), shows that the main mechanism implicated in this type of thermophoresis is the thermal expansion of the fluid, and that the clusters migrate to hotter regions with a characteristic thermal diffusion coefficient D_T of 9×10^{-7} cm^2 K^{-1} s^{-1}. We further show that the characteristic length associated with thermophoresis is not that of the nanotube clusters size, $O(1)$ μm, but that corresponding to the microstructure of the clusters, $O(1)$ nm. We finally discuss the role of the formation of gas−liquid interfaces (microbubbles) at high optical powers on the deposition of carbon nanotubes on the optical fiber end faces.

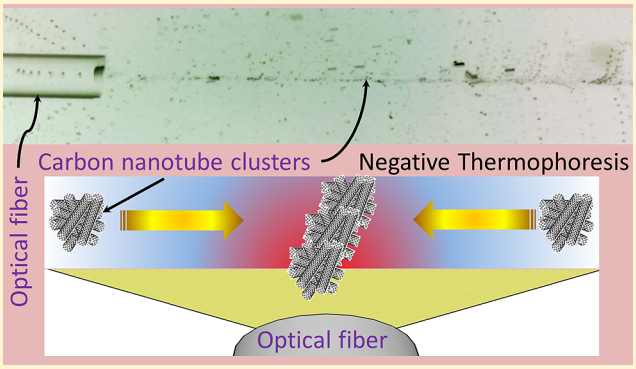

INTRODUCTION

In the realm of hydrodynamics and surface phenomena, it is possible to study micro- and macrosystems indistinctively if one considers the right scale parameters. Such is the case for the Reynolds and Bond numbers criteria. There are, however, other set of phenomena that appear exclusively at the microscale without having analogous macroscaled counterparts. Typical examples of these are the Brownian and phoretic motions.[1−3] Phoretic transport has received especial interest because it allows the manipulation, characterization, separation or increase of concentration (against diffusive transport) of many kinds of particle dispersions, including colloidal, macromolecular or living cell suspensions.[4−8] Prediction of the particle's migration velocity usually requires the knowledge of specific interactions with the surrounding liquid,[9−11] and sometimes even different types of transport pathways may participate in a single experimental realization.[12] For example, if one uses laser beams to manipulate particles, the electromagnetic radiation can induce motion either by direct momentum transfer or by triggering different heat transfer modes due to light absorption. The goal of the present paper is to distinguish the different transport mechanisms implicated in the motion of multiwalled carbon nanotube (MWCN) dispersions in liquids irradiated by a laser beam. We aim at elucidating the origin of the thermophoretic motion of the MWCN clusters using interfacial transport theory. We pursued as well in identifying the roles of radiation pressure and convection currents on the motion of such dispersions.

Thermophoresis refers to the particle motion in response to a temperature gradient, and it considers motion either toward the colder (positive thermophoresis) or hotter (negative thermophoresis) regions.[9,13] It is characterized by a thermal diffusion coefficient D_T, which is usually scaled by the common diffusion coefficient D yielding the so-called Soret coefficient $S_T = D_T/D$. In the case of charged colloids, the mechanisms implicated in thermophoresis are usually explained in terms of thermodynamic functions, such as the entropic cost of maintaining the structure of the electrical double layer at a

Received: July 2, 2015
Revised: August 21, 2015
Published: August 26, 2015

DOI: 10.1021/acs.langmuir.5b02448
Langmuir 2015, 31, 10066−10075

given temperature.[14−16] In the case of noncharged particles, the thermophoretic velocity has been estimated by solving the flow generated in the interfacial layer by means of particle−solvent interactions.[9,10,13] If such interactions between particle and solvent are important in describing thermophoresis in such kinds of systems, it has been further shown that thermal expansion of the fluid due to local temperature increments is as important as the interaction potentials. The argument of Brenner and Bielenberg[17] that thermophoresis is just a result of a background "volume velocity" of the fluid due to thermal expansion has shown to be valid in some experiments.[12] In this report we found, as Brenner and Bielenberg[17] and Semenov and Schimpf,[10,18] that thermal expansion is indeed the most important driving mechanism of the thermophoretic motion observed in this work.

We must mention that other mechanisms have been proposed as well to explain thermophoresis in noncharged particle suspensions.[11,19−21] Würger,[11] for example, conceived thermophoresis of soft particles as a scaled version of the thermocapillary flow, where surface tension gradients constitute a key factor in defining the particle velocity.

Photophoresis and Radiation Pressure. These two phenomena are generated by the same effect: electromagnetic radiation, usually in the form of a coherent laser beam, impinging on a particle having a different complex refractive index with respect to the surrounding medium.[22] It is actually a common practice to use both terms indistinctively.[23,24] However, in this work we adopt the original meaning for each term in order to emphasize their difference. Radiation pressure is the direct momentum transfer from electromagnetic radiation to a surface interacting via light absorption or reflection.[22] For instance, in the case of a plane light wave, the force exerted on a spherical particle with radius r_0 via light absorption is[22]

$$F_{rad} = \frac{\pi {r_0}^2 I_o}{c}\left[1 - \frac{{\mathcal{L}_{abs}}^2}{2{r_0}^2} f\right] \quad (1)$$

where $f = 1 - (1 + 2r_0/\mathcal{L}_{abs})\, e^{-2r_0/\mathcal{L}_{abs}}$. Here I_o is the incident optical intensity, c the speed of light, and $\mathcal{L}_{abs} = {\kappa_{abs}}^{-1}$, where κ_{abs} is the absorption coefficient of the particle. The derivation of this formula relies on the simple assumption that the power per unit area absorbed by the particle obeys the Beer−Lambert law, where the zero and maximum optical lengths lie on the surface and center of the spherical particle, respectively.

Besides motion generation, part of the absorbed light is usually dissipated as heat in the surrounding medium. If the particles are suspended in a gas, this increase in temperature rises the kinetic energy of the gas molecules, and since the incident radiation is nonevenly distributed on a spherical particle, there will be an asymmetric distribution of pressure in the gas that will ultimately move the particle on a resultant direction: this is what is known as photophoresis[22,25,26] and constitute the thermophoretic version in gases.[13] It has been observed that photophoresis actually overcomes, by several orders of magnitude, the effects of radiation pressure in aerosols and nanofoams (particle dispersions in gases).[22,26] We will show, on the other hand, that photophoresis does not play any significant role in the motion of particles in liquids. It is worth mentioning that Soong et al.[27] have used the term "photophoresis" to denote a variety of thermophoresis in liquids in which the temperature gradient is generated by the particle itself thanks to light absorption. The formulation of their proposal, which uses the so-called asymmetry factor for spherical particles, is capable to predict either positive or negative Soret coefficients. In this work, we will see that the regular thermophoresis (temperature gradients imposed by the liquid) suffice to explain the observed motions of the MWCN clusters.

In the following section, we will describe the experimental setup used to study the motion of MWCN clusters followed by the main results of this work. The Discussion section includes a theoretical description of thermophoresis based on interfacial motion and a new velocity equation is obtained in order to explain thermophoresis in these kinds of dispersions. We conclude the discussion by pointing out the role of the formation of gas−liquid interfaces at high optical powers on the deposition of MWCN on optical fiber end faces.

EXPERIMENTAL SECTION

Multiwalled carbon nanotubes (Sigma-Aldrich, O.D. of 6−9 nm) were dispersed in water or ethanol at a concentration of 2 ppm; the suspensions were sonicated for 8 min before experiments. These highly diluted dispersions were prepared in order to avoid the formation of dense clusters and overheating of the visualization cell. The suspensions were placed in a 1 × 1 cm^2 cell placed between a microscope slide and coverslip using 150 μm mica sheets as spacers. An optical fiber (Corning SMF-28e, numerical aperture NA = 0.14) with diameters of 8.2 and 125 μm in core and cladding, respectively, was introduced through a lateral wall and placed at the center of the cell. The optical fiber was connected to two laser diodes, one emitting at 975 nm and another at 1550 nm in order to test the motion of the MWCN clusters at two optical wavelengths. In order to ensure a single-mode output with a Gaussian intensity profile, a mode stripper was used near the output end of the fiber. Since the laser beam was not collimated, the optical intensity varies with the distance with respect to the fiber tip. Hence, most of the measurements were done at a distance of $d \sim 500$ μm from the fiber tip, which corresponds roughly to the distance at which the laser cone attains an area corresponding to that of the fiber end face.

It is well-known that carbon nanotube dispersions in polar solvents tend to cluster,[28,29] this feature allowed us to visualize the motion of individual clusters using a digital microscope (DinoLite AD7013MZT) placed perpendicularly to the cell plane and having a typical resolution of 1 μm/pixel. Tan et al.[30] have shown that it is possible to quantify the collective motion of individual carbon nanotubes employing fluorescence microscopy and using functionalized nanotubes to improve their dispersion in polar solvents. We do not, however, pursued such experimental treatment in this work. The average size of the clusters was estimated by image processing in MatLab while particle tracking was performed with ImageJ. Typically, the motion of the clusters was very slow to observe a significant displacement in a real time movie; we therefore decided to take pictures of the dispersion every minute for time periods ranging from 12 to 60 min and then obtain the displacements by superimposing the individual images.

RESULTS

Figure 1a shows a "panoramic" photo of the MWCN dispersion formed in ethanol. The picture shows the general trend observed in all the experiments (for both wavelengths and both liquids): the MWCN clusters travel toward the laser axis forming an entangled array some distance apart from the fiber tip. Similar arrays have been observed in other kinds of suspensions using optical fibers as well.[31] The average equivalent cluster radius in ethanol was found to be 2.4 μm, while in water it was 6 μm. Figure 1b and c shows

DOI: 10.1021/acs.langmuir.5b02448
Langmuir 2015, 31, 10066−10075

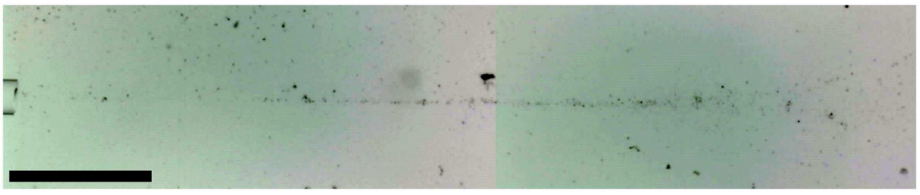

(a) MWCN in ethanol, 1550nm, 16.5mW. Scale bar is 500μm

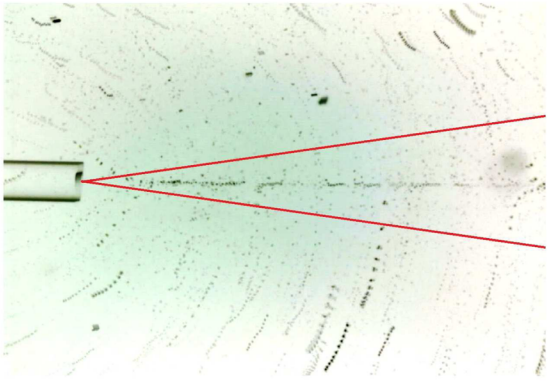

(b) MWCN in ethanol, 975nm, 71.4mW

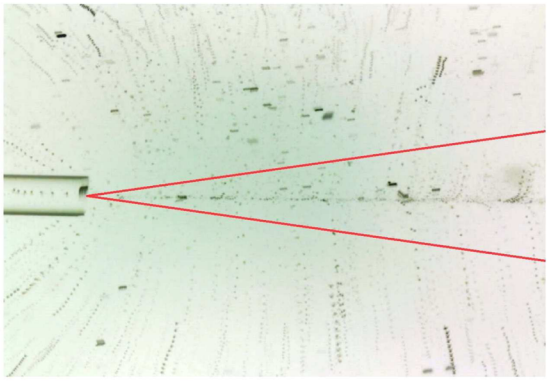

(c) MWCN in ethanol, 1550nm, 10.1mW

Figure 1. Pictures showing the dispersion of MWCN clusters in ethanol: (a) Joined images showing the overall length of the clusters arrayed under laser irradiation; the optical fiber tip can be seen at the left side. (b,c) Superimposed images showing the cluster displacement for two different laser wavelengths. The images are acquired 1 min apart. The red lines illustrate the light cone at the output of the fiber (approx. 6°), calculated with the numerical aperture of the fiber ($\sin^{-1}[0.14/n_i]$, with n_i being the refraction index of the fluid).

superimposed images acquired 1 min apart in order to visualize the displacements of the clusters for two laser wavelengths. Clearly, the particles tend to group along the laser beam axis. The red lines illustrate the divergence cone of the laser beam drawn according to the numerical aperture of the fiber. It is important to note that motion occurs both, inside and outside the laser cone, hence, motion is driven by direct laser irradiation but also by thermal effects. If we look carefully at images b and c, an interesting difference is observed between the motion produced using a wavelength of 975 nm and that produced with the laser operating at 1550 nm. In both cases and at short distances from the fiber tip, the clusters tend to move away from the fiber end face. Notice however that farther away from the fiber tip, the trajectories of the clusters differ in direction: while for 975 nm the clusters move away from the laser tip, the opposite occurs with the 1550 nm light source (see the right side of Figure 1b and c). These differences arise from the interplay between thermophoresis and radiative pressure in the region located inside the laser cone, the first dominating at 1550 nm owing to a stronger optical absorption in the liquids at this wavelength (see Table1), and the last one dominating at 975 nm due to strong absorption of the carbon

Table 1. Comparative Chart of the Relevant Physical Parameters for Water and Ethanol

parameter		water	ethanol
MWCN cluster radius	r_0	6 μm	2.4 μm
absorption coefficient at 975 nm[38]	κ_{abs}	40 m^{-1}	6 m^{-1}
absorption coefficient at 1550 nm[38]		900 m^{-1}	550 m^{-1}
surface tension temperature coeff.[39]	σ_T	−0.1477 mN/m·K	−0.0832 mN/m·K
thermal expansion coeff.	α_v	2.07×10^{-4} K^{-1}	7.5×10^{-4} K^{-1}

DOI: 10.1021/acs.langmuir.5b02448
Langmuir 2015, 31, 10066−10075

clusters at this wavelength.[32] In the Supporting Information, we have included a fast-motion video of the clusters dispersed in water (60 frames taken in 1 h are shown in 5 s, 975 nm, 71.4 mW).

Figure 2 shows the mean velocity as a function of the optical power registered at different positions with respect to the laser

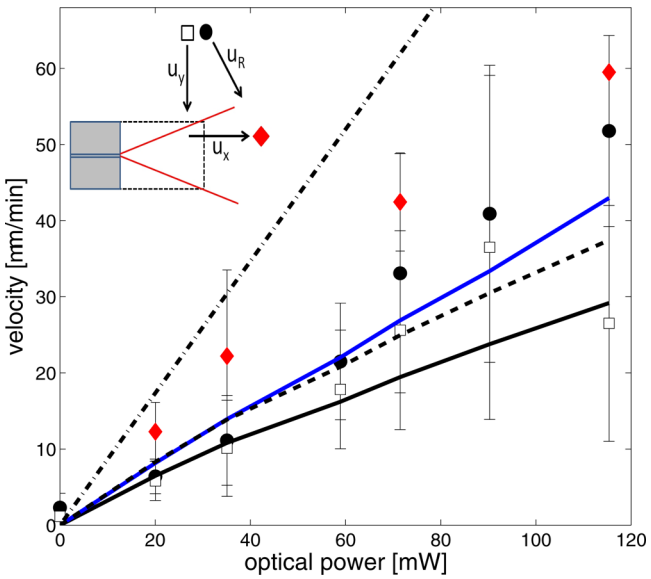

Figure 2. Mean velocity as a function of the optical power registered at different locations with respect to the laser cone (see inset). Data correspond to the clusters dispersed in ethanol irradiated with the laser of 975 nm; (solid black circle) resultant mean velocity u_R measured outside the laser cone; (open square) y-component, u_y, of u_R; (sold red diamond) x-component, u_x, of the mean velocities measured inside the laser cone. The lines correspond to theoretical values: the solid black line corresponds to eq 14 derived in this work for thermophoretic transport; the blue solid line corresponds to the added contributions of thermophoresis and convective flow; the dashed line corresponds to Würger solution, eq 16, for thermophoresis driven by thermocapillary flow;[11] the dotted-dashed line corresponds to the motion produced by radiative pressure; i.e., eq 1 equated with the Stokes drag force.

cone (see the inset in Figure 2) for clusters dispersed in ethanol. Circular symbols in Figure 2 correspond to the resultant velocities measured outside the laser cone and can give a direct measurement of the thermophoretic velocity. The square symbols correspond to the y-component of such velocities. The diamonds correspond to the x-component of the velocities measured inside the cone and can give an estimate of the motion produced by radiative pressure. The maximum velocities registered in the experiments were around 1 μm/s. Note that the y-components of the velocities are close to the resultant velocities except for the highest optical powers. This indicates that the motion of the MWCN clusters is mainly directed toward the beam axis. The lines in the figure correspond to theoretical values and are discussed in the next section.

Figure 3 shows a case of study where the velocities obtained in ethanol and water are compared. We can see clearly that, for the two wavelengths used, 975 and 1550 nm, the cluster velocities are higher in ethanol than in water. Such differences in velocities, which depend mainly on the kind of liquid used, turned out to be a key observation that helped us define the mechanism implicated in the thermophoretic motion, as discussed in the next section.

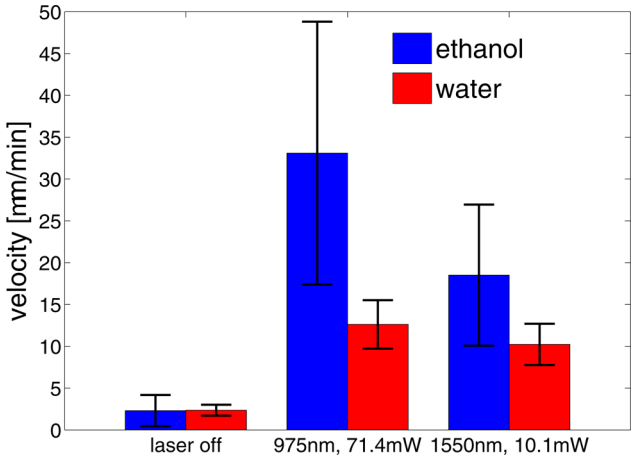

Figure 3. Comparative graph showing the cluster velocities obtained in two polar solvents: ethanol and water.

At this point, one may argue that besides thermophoretic and radiation pressure effects, optical intensity gradients and convective currents could impose as well a net motion on the MWCN clusters. Indeed, it has been shown that carbon nanotubes can be trapped by optical intensity gradients at similar wavelengths as those employed in this work.[30,33] On the other hand, local increments of the temperature inside a fluid always produce convection currents due to the density dependence on T, which certainly may compete with the transport induced by thermophoresis if the cell height is not small enough.[34]

In order to estimate the optical trapping contribution on the clusters velocities, as a first approximation, we equate the optical gradient forces with the Stokes drag force:

$$\frac{\alpha \nabla I(\hat{x})}{n_i \epsilon_0 c} = 6\pi\eta r_0 U \tag{2}$$

where α is the polarizability of the MWCN clusters, n_i is the refraction index of the fluid and ϵ_0 is the free space permittivity. If we assume that the laser beam has a Gaussian intensity profile, it is easy to show that the maximum intensity gradient in the radial direction is

$$\nabla_r I_{\max} = -\frac{4P_o}{w^3\pi} e^{-1-\kappa_{abs}y} \tag{3}$$

where κ_{abs} is the absorption coefficient of the solvent, w is the laser beam radius, and P_o is the optical power. We took the value of α from ref 35, which for an infinite 3D array of carbon nanotubes α has a theoretical value of 479 Å^3 ($\sim 6 \times 10^{-38}$ C^2 m^2 J^{-1} in SI units). Therefore, in ethanol (n_i = 1.36, other physical parameters are listed in Tables 1 and 2), at a depth of $\sim$500 μm from the fiber tip, having a beam radius of 50 μm and an optical power of 115.3 mW, the estimated maximum particle velocity due to optical trapping is about 1×10^{-8} μm/min, evidently too small compared to the experimental values shown in Figure 2. Hence, unlike those situations in which the laser beam is collimated or focused, here the divergent cone of the laser beam produce negligible trapping force. We can confidently say, therefore, that MWCN aggregation at the beam axis is solely due to thermophoresis.

We now focus on the convection flow issue. In order to obtain the flow field and the temperature profiles inside the cell, we solved numerically the 3D Stokes equations together with

DOI: 10.1021/acs.langmuir.5b02448
Langmuir 2015, 31, 10066−10075

Table 2. Relevant Physical Parameters for Ethanol and for the Repulsive Potential, Eq 13[a]

viscosity	μ	0.9 mPa·s
molecular volume	ν_o	98.7 Å^3
thermal conductivity	k_s	0.15 W/m·K
thermal diffusivity	α_T	0.07 mm^2/s
Hamaker constant	$\mathcal{H}$	4.2×10^{-20} J
interaction potential constant	C	1×10^{-20} J
hydrophobic characteristic length	λ_r	1 nm^{-1}

[a]The molecular volume was calculated as $\nu_o = PM/\rho N_A$, where for pure ethanol the molecular weight is PM = 46.07 g/mol, the density ρ = 0.775 g/cm^3, and N_A is the Avogadro number.

the steady heat transfer equation using the Fluid Flow > Nonisothermal laminar flow package of COMSOL Multiphysics 5.0. We included a heat generation term Q of the form:

$$Q = \frac{2\kappa_{abs}P_o}{w^2\pi}\exp\left[-\frac{2(x^2+z^2)}{w^2} - \kappa_{abs}y\right] \quad (4)$$

where $w = 2.7\ [\mu m] + (\tan 6°)y$ due to the numerical aperture of the optical fiber. An example of the velocity profiles obtained in ethanol for P_o = 115.3 mW (λ = 975 nm) is shown in Figure 4 (left image). The domain dimensions were 0.15 × 1 × 1 mm^3, and the fluid was sandwiched between two layers of glass surrounded by air. We can see that the velocities develope horizontal "8" shaped profiles that evinced the formation of convection currents near the fiber axis. The figure at the right side shows in detail the x-component of such velocities at a depth of y = 442 μm with respect to the fiber tip. It is evident that, close to the fiber axis, convection is high enough to move the particles at speeds similar to those reported in Figure 2. However, at distances larger than two fiber diameters ($2D_{fib}$ in the figure), the velocities are by much 14 μm/min. We therefore can assert that while MWCN aggregation at the beam axis is due exclusively to thermophoresis, its motion is a combination of thermophoretic and convection currents effects; later we will show that the former dominates the motion at low optical powers. With this numerical calculation, we also obtained the increments in temperature $\Delta T = T_{max} - 300$ [K], as well as the temperature gradients for a certain P_o value. These were calculated assuming that the gradients have a linear profile, that is, that $\nabla T = \Delta T/L$, where L = 5 mm is the approximated distance between the fiber tip and the cell walls in the experimental setup.

DISCUSSION

Motion Outside the Laser Cone. Once we have define that the motion observed in this region is caused by temperature gradients alone, we will discuss now the nature of the negative thermophoretic motion observed for the MWCN clusters in polar solvents. It is well-known that carbon nanotubes (graphene lattices) have hydrophobic interactions with polar solvents such as water or ethanol.[36,37] The surface tension gradient mechanism, as explained by Würger,[11] is therefore a good candidate to explain the motion observed here since the carbon nanotube-solvent interactions generate a gas/liquid-like interface, as suggested by several molecular dynamic simulations.[36,37] This explanation will not, however, support the experimental results since water has a larger surface tension

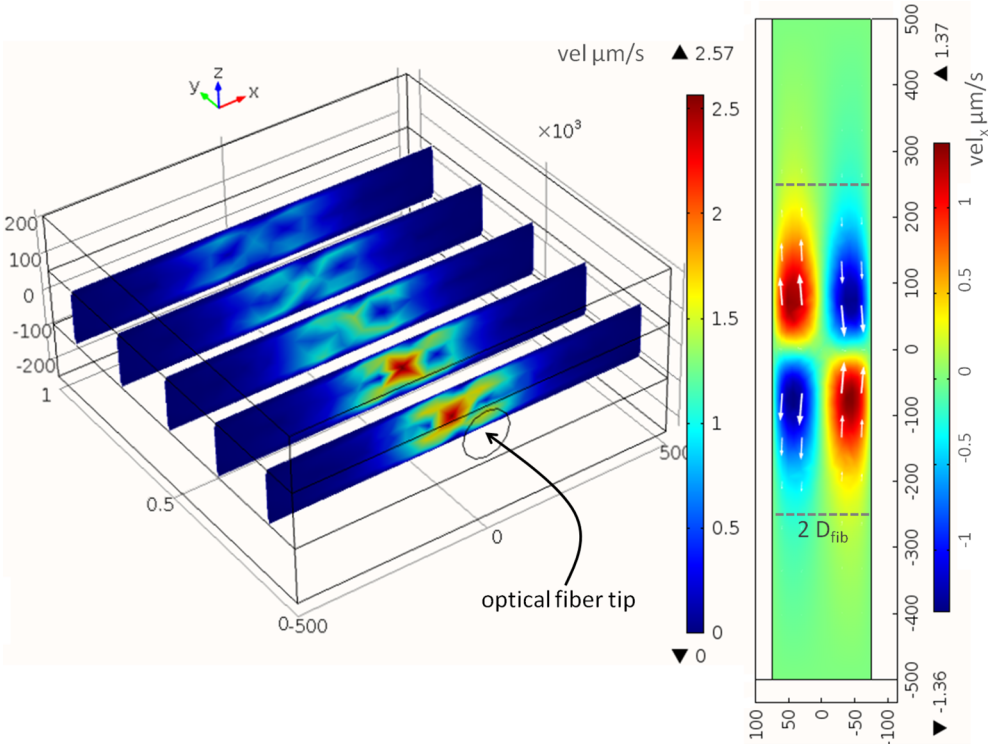

Figure 4. Numerical solutions of the velocity profiles obtained in ethanol irradiated by a 975 nm divergent laser beam; P_o = 115.3 mW. The fluid domain consists of a 0.15 × 1 × 1 mm^3 box surrounded by glass with the same thickness, the y-coordinate coincides with the beam axis. The figure at the left shows a 3D view of the velocity profiles, while the figure at the right side denotes the x-component of the velocities inside the cell. $2D_{fib}$ refers to a distance two fiber diameters (2 × 125 μm) away from the cell center. The ΔT obtained in these numerical calculations ranged from 6 to 27 K and ∇T from 1.4 to 8.5 K/mm, with both displaying a linear relation with P_o.

DOI: 10.1021/acs.langmuir.5b02448
Langmuir 2015, 31, 10066−10075

temperature coefficient than ethanol (see Table 1), and will therefore produce larger displacements, contrary to what is observed in the experiments.

The other possible mechanism provided for nonionic particles is the thermal expansion of the solvent mediated by particle−solvent interactions:[10,17,18,40] this will be analyze in detail in the following sections. The theoretical background that we are going to use corresponds to that developed by Semenov and Schimpf.[10,18] The equations that they obtained were specifically for the case of attractive interactions between the particle and the solvent. Here we are going to extend the theory to general interaction potentials.

Following the hydrodynamic approach, the starting point of the theory consists of writing the equations of motion at the interface using the thin film approximation. If we employ local

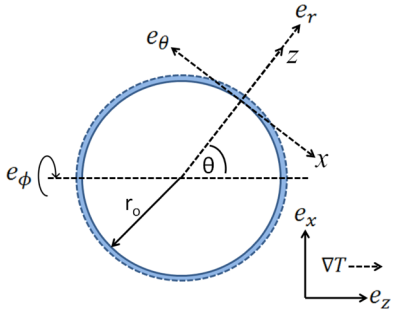

Figure 5. Coordinate systems used to solve for the particle velocity U: e_x, e_z are fixed spatial coordinates. Note that for the present problem $\nabla T = \nabla T_z e_z$. e_r, e_θ, e_ϕ are spherical coordinates attached to the particle with radius r_o. x, z are local coordinates relevant to the flow generated at the interface, represented in blue color.

coordinates attached to the particle (x, z; see Figure 5), the Stokes equations can be written as

$$\mu \frac{\partial^2 u_x}{\partial z^2} = \frac{\partial p}{\partial x} - \frac{f_x}{\nu_o} \tag{5}$$

$$0 = \frac{\partial p}{\partial z} - \frac{f_z}{\nu_o} \tag{6}$$

where f is a body force due to particle−solvent interactions and ν_o is the specific volume occupied by the liquid molecule and which has replaced the number density since the system is "saturated" by the solvent.

If we consider an interaction potential of the form $f = -\nabla\Phi$, from eq 6, we get that $p = -\Phi/\nu_o$. If we consider only the contribution of such conservative force f, after substituting the value of the pressure in eq 5, we observe that the right-hand side becomes zero due to the hydrodynamic equilibrium condition ($\nabla p - f/\nu_o = 0$). Therefore, the key point is to consider that the specific volume ν_o is subject as well to spatial variations upon imposing a certain temperature gradient. In this way, the derivative of $p = -\Phi(\hat{\mathbf{r}})/\nu_o(\hat{\mathbf{r}})$ came out to be

$$\nabla p = \frac{1}{\nu_o}[\Phi\alpha_\nu \nabla T - \nabla\Phi] \tag{7}$$

where α_ν is the thermal expansion coefficient of the solvent, defined as $\alpha_\nu = \partial \ln(\nu_o)/\partial T$. After substituting this relation in eq 5, we get the equation of motion in its thermophoretic version:[18]

$$\mu \frac{\partial^2 u_x}{\partial z^2} = \frac{\Phi\alpha_\nu}{\nu_o} \frac{\partial T}{\partial x} \tag{8}$$

The term on the right-hand side can be interpreted as an excess pressure gradient at the interface, $\partial_x p^* = \Phi\alpha_\nu(\partial T/\partial x)/\nu_o$, and has the following consequence: for attractive interaction potentials ($\Phi < 0$), a ∇p^* is established against the temperature gradient ∇T, which produces an interfacial flow in the direction of ∇T as seen from the particle frame of reference (see Figure 6). This results in a particle migration toward $-\nabla T$, that is,

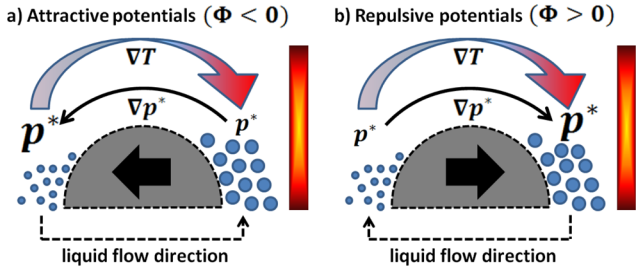

Figure 6. Scheme showing the potential Φ dependent relation between interfacial pressure and temperature gradients in eq 7. The vertical red bars denote a heat source while the gray semicircles denote half of a particle immersed in a fluid. The blue circles represent a mesoscopic volume of the liquid that increases near the hotter region due to thermal expansion; p^* represents a hydrodynamic pressure at the interface and liquid flows, as usual, from higher to lower values of p^*. In the case of attractive potentials (a), the direction of ∇p^* makes the particle migrate to colder regions, where the specific volume of the liquid ν_o is found to acquire a minimum value. In the case of repulsive potentials (b), the direction of ∇p^* makes the particle migrate to hotter regions, where ν_o finds a maximum value.

toward colder regions, as seen from the laboratory frame of reference. Exactly the opposite effect will happen if the potentials are repulsive in nature; that is, the particle will migrate toward the hotter regions (see Figure 6). This mechanism has an implicit thermodynamic principle and is related to a free energy minimization: for attractive potentials, the particles migrate to colder regions because maximum interactions per unit area with the solvent will occur there, that is, ν_o has a minimum. Conversely, in the case of repulsive potentials, the particles migrate to hotter regions because it is there where it finds the minimum interactions/area with the solvent; that is, ν_o has a maximum. Thus, we can see that the particle motion is driven by spatial variations of the molecular volume ν_o, but its direction is determined by the sign of the interaction potential. The same relation between motion direction and interactive potentials was found by Derjaguin using a different approach.[1,41]

Once we have shown how ∇p^* produces an interfacial flow, we proceed to calculate it by double integration of eq 8, which yields $u_x = -1/\mu \int_0^\infty \partial_x p^* z\, dz$. It is well-known that interfacial motion can also be generated if interfacial stresses act on a deformable surface, that is, if there is a characteristic slip length l. Morthomas and Würger[42] have considered the contribution of such interfacial stresses, given by $\tau = -\int_0^\infty \partial_x p^*\, dz$ (the negative sign comes from the definition of the interfacial stress, which is zero at $z \to \infty$ and attains a maximum value at $z = 0$), to the slip velocity u_s:

$$u_s = \frac{u_x + l\tau/\mu}{1 + 2l/r_o} \tag{9}$$

DOI: 10.1021/acs.langmuir.5b02448
Langmuir 2015, 31, 10066−10075

Once the slip velocity u_s is known, the flow field in the liquid bulk can be computed using u_s as the boundary condition. Here we are only concerned in calculating the particle velocity U, which is obtained by changing form the particle frame of reference (x,z) to the fixed frame of reference (e_x,e_z), that is:

$$U = -\langle u_s \rangle \tag{10}$$

where $\langle ... \rangle = 1/4\pi \int_0^{2\pi} \int_0^{\pi} \sin\theta (...) d\theta\, d\phi$ is the orientational average of the slip velocity,[11] which can be computed using the relation $x = -\cos\theta e_x + \sin\theta e_z$ (see Figure 5). In order to compute $\partial_x T$ in eq 8, we have considered the temperature field formed around a spherical particle:[10]

$$T = T_o + \nabla T r_o \cos\theta \left(\frac{r}{r_o} + \frac{1-n}{n+2} \frac{r_o^2}{r^2} \right) \tag{11}$$

where $\nabla T = \nabla T_z e_z$ is an overall thermal gradient in the liquid, which is assumed to be stationary, T_o is the temperature at the center of the particle, and $n = k_p/k_s$ is the particle to solvent thermal conductivity ratio. The temperature gradient along the interface is therefore given by

$$\left.\frac{\partial T}{\partial x}\right|_{\text{interface}} \approx -\frac{1}{r}\left.\frac{\partial T}{\partial \theta}\right|_{r=r_o} = \frac{3}{n+2}\nabla T \sin\theta \tag{12}$$

The last term we need to define is the interaction potential Φ. As mentioned above, dispersions of carbon nanotubes in polar solvents are characterized by having hydrophobic interactions.[36,37] This repulsive potential is a result of several interactions occurring at the interface and include contributions from carbon−carbon interactions, solvent−solvent molecule interactions such as hydrogen bonds, and carbon−solvent interactions including van der Waals forces.[36] Despite the complicated description that characterize these systems, it is somewhat accepted that hydrophobic interactions decay exponentially with the intermolecular distance.[43] We therefore assume a very simple phenomenological repulsive potential of the form:

$$\Phi = C\, e^{-\lambda_r z} \tag{13}$$

We have assigned to C a value of 1×10^{-20} J, which originally corresponds to the value of methane−methane attractive interactions in water.[43] For $1/\lambda_r$, we designated a value of 1 nm, which has been observed to be a representative value for the characteristic decay length of hydrophobic interactions.[43] Taking into account eqs 8−10, 12, and 13, we finally obtain the thermophoretic velocity for the system as

$$U = \frac{2\alpha_v C}{\mu \nu_o (n+2)\lambda_r^2}\left[\frac{1+l\lambda_r}{1+2l/r_o}\right]\nabla T \tag{14}$$

The values of the constants appearing in this equation are listed in Tables1 and 2. Note that the particle velocity points in the same direction as the temperature gradient, i.e., the particle moves toward the hotter region. In order to compare eq 14 with the experiments, we estimated ∇T from the numerical simulations, as mentioned above. The solid black line in Figure 2 corresponds to the theoretical velocity, eq 14, for clusters immersed in ethanol using $n = 1$ and $(1 + l\lambda_r)/(1 + 2l/r_o) = 1.6$; eq 14 therefore estimates a thermal diffusion coefficient of 9×10^{-7} cm^2 K^{-1} s^{-1} for the MWCN−ethanol system. The assumption that the thermal diffusivity of ethanol and carbon nanotubes are equal, that is, $n = 1$, seems to be flawed, since the thermal diffusivity of the latter is at least 3 orders of magnitude higher than that the former. Recall, however, that the moving entities seen in Figure 1 are not solid particles but clusters of nanotubes embedded by the solvent. In the case of carbon nanoparticles dispersed in air (nanofoams),[44] for example, the effective thermal conductivity of the foams was considered to be that of air, which constitutes the limiting conductivity. We have assumed the same behavior for dispersions made in liquids. Another interesting feature is that the $(1+l\lambda_r)/(1 + 2l/r_o)$ term is of $O(1)$; this in turn has an interesting interpretation, as discussed below. Suppose that we consider that the slip length of the nanotubes-solvent system is indeed very high due to the nature of the interaction potential; then the terms in eq 14 involving l become:

$$\left.\frac{1+l\lambda_r}{1+2lr_o}\right|_{l\to\infty} = \frac{\lambda_r r_o}{2} \tag{15}$$

If we consider r_o to be the size of the cluster, $O(1)$ μm, then the actual theoretical values will be multiplied by a factor of $\sim 10^2$, resulting in very high velocities with respect to the experimental values. However, if r_o takes the value of a characteristic microstructure length, say the MWCN radius of $O(1)$ nm, then the term $\lambda_r r_o/2$ becomes of $O(1)$. These length scales imply two important characteristics for the present system: the first one is that the observed motion is not produced by interfacial (thermocapillary) stresses, which correspond to the limit where $l \to \infty$.[42] The MWCN-ethanol interface behaves rather as a solid−liquid interface having a finite slip length. The other important feature is that the relevant length scale for thermophoresis does not corresponds to the cluster size itself but rather on the microstructure length of the clusters. In terms of the recent work published by Morozov and Köhler,[45] this means that thermophoretic motion happens in a thin outer layer of the cluster, while the core behaves as a nondraining medium that do not participate in thermophoretic mechanisms. Considering that the MWCN have a mean radius of $r_o = 3.75$ nm, for $\lambda_r = 1$ nm^{-1} a slip length of $l = 4$ nm yields the factor 1.6 mentioned above.

In Figure 2, we have also included the total velocity (blue line) achieved if the theoretical thermophoretic velocity is added with the x-component of the convective velocity at a distance $2D_{fib}$ away from the cell center (see Figure 4). It becomes clear that convective currents appear to be important only at high optical powers, where its velocity become as high as the thermophoretic one. Near the optical fiber axis, on the other hand, an accelerated motion is expected to occur in all cases due to highly local convection currents.

In order to compare our results with other theoretical formulations, we have computed the thermophoretic velocity as given by Benner and Bielenberg,[17] which also considers the effects of the liquid thermal expansion but without considering any particle−solvent interactions; we computed as well the thermophoretic velocity driven by Marangoni effects as given by Würger.[11] The Brenner−Bielenberg equation states that $U = -\alpha_T \alpha_v \nabla T/(1 + n/2)$, where α_T is the thermal diffusivity of ethanol (see Table 2) and again we have assumed that $n = 1$. This equation gives the correct order of magnitude of the thermophoretic velocity upon comparing with the experiments; however, the direction of U is opposite to that seen in the experiments and actually the Brenner−Bielenberg equation dictates that thermophoresis will always occur in one direction: toward the colder regions. We therefore highlight the comment

DOI: 10.1021/acs.langmuir.5b02448
Langmuir 2015, 31, 10066−10075

that although the purely continuous approach followed by Brenner and Bielenberg is correct in its own terms, in thermophoretic motion we simply cannot ignore noncontinuum considerations, that is, molecular interaction potentials and interfacial displacements.

The thermophoretic velocity driven by thermocapillary flow has the form:[11]

$$U = -\frac{\sigma_T r_o}{3\mu}\nabla T \tag{16}$$

where σ_T is the surface tension temperature coefficient; see Table 1. If we assume again that r_o takes the microstructure representative value of 3.75 nm, in connection with the nondraining core argument of Morozov and Köhler,[45] eq 16 also gives the correct magnitude, and direction, of the thermophoretic velocity, as seen in Figure 2 (dashed line); the correspondence is actually very good even though we have considered the original surface tension temperature coefficient of ethanol as is given in Table 1 for a liquid−gas interface. Agreement between experiments and both equations, 14 and 16, gives us the possibility to reconcile the hydrophobic interaction perspective taken in this work, with the surface tension driven mechanism proposed by Würger. As mentioned above, however, the only reason we have decided to adopt the liquid thermal expansion mechanism rather than micro-Marangoni effects (and thus assume that the system has as a solid−liquid interface), is because eq 16 will predict higher values of U in water than in ethanol, contrary to the experimental observations (Figure 3).

Motion inside the Laser Cone: Radiative Pressure Effects. We have seen in Figures 1 and 2 (red diamonds) that when the clusters enter the laser cone, they are expelled in the direction of the beam. The dashed-dotted line in Figure 2 corresponds to the velocities calculated using eq 1, that is, equating the radiative pressure with the Stokes drag force $F_S = 6\pi\mu r_o U$. Here μ is the viscosity of ethanol (Table 2), I_o was calculated at a distance $d = 442$ μm away from the fiber tip, the absorption length of the carbon nanotubes was considered to be $\mathcal{L}_{abs} = 40$ μm,[22] and r_o assumes this time the cluster radius, which corresponds to the total area irradiated by the electromagnetic radiation (external force). Equation 1 then gives an upper bound to the velocity produced by a Gaussian laser beam by means of radiative pressure. Again, the theoretical velocities match the order of magnitude of the experimental data ($O(1)$ μm/s). Note in addition that the theoretical and experimental velocities along the fiber axis are slightly higher than the lateral, thermophoretic velocities. Similar to the later case, we expect that convection currents will impact in some degree the velocities along the fiber axis at high optical powers.

Motion at High Optical Powers. It has been well documented that when the optical power output is high enough, strong convective currents appear and heating of the absorbing particles can produce microbubbles in the liquid; this bubbles, in turn, migrate toward the light source by thermocapillary flow at the gas−liquid interface and are implicated in the deposition of particles on the surface of the light source.[46−48] This short section supports these experimental results and discards any contribution from phoretic transport in the deposition of nanoparticles (in fact, radiative pressure keeps away the nanotubes from the fiber tip, as we saw in the experiments). Figure 7a shows a bubble attached to the fiber tip (109 mW). The thermocapillary flow on the bubble surface generate a pair of quasi-2D microvortices at both side of the fiber. The vortices are around 360 μm in diameter and can be seen thanks to the superposition of images taken at different times. The tangential velocity of the vortices is much higher than any velocity obtained in the transport described in sections above and is around 1.7 mm/s. Figure 7b shows a sequence of images of a bubble approaching the fiber tip due to thermocapillary forces; it carries with it an adsorbed nanotube cluster (red arrow in Figure 7b), which ultimately reaches the fiber thanks to the transport mediated by the bubble. This is clear evidence that the deposition of carbon nanotubes is mediated by the formation of a gas−liquid interface. Once the nanotubes are deposited over the fiber surface, some attractive forces between the nanoparticles and the fiber surface must come into play in order to allow a long-term deposition, as revealed by some experiments.[49] This argument may sound reasonable if one considers that the nanotubes and the fiber surface contact each other having a gas phase in between.

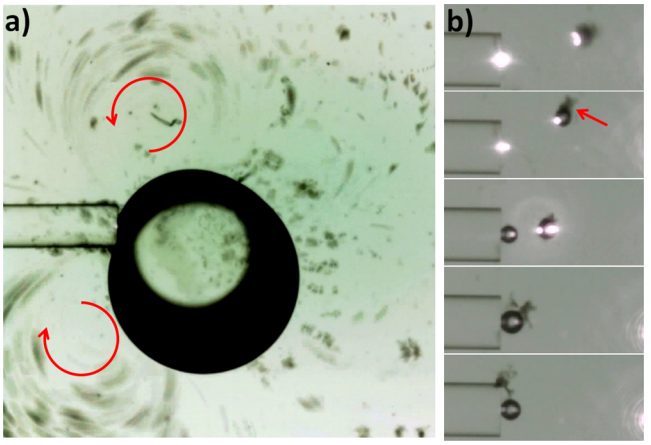

Figure 7. Formation of a gas−liquid interface at high optical powers. (a) Superposition of images taken at different times showing a pair of quasi-2D microvortices formed at the optical fiber tip thanks to the thermocapillary flow generated at the bubble surface (975 nm, 109 mW). Note that the gas−liquid interface moves to the right, i.e., to colder regions, where surface tension attains a maximum value. Red arrows denote the direction of rotation of the vortices. (b) Sequence of images showing a bubble moving toward the fiber tip and carrying with it a MWCN cluster, indicated with the red arrow (975 nm, 115 mW). Note that the bubble coalesce with another one that forms meanwhile at the fiber surface. The image sequence covers a total period of 5 s.

The combination rule of the Hamaker constant (van der Waals attractive potentials) between medium 1 and 3 interacting across medium 2 is written as[43] $\mathcal{H}_{123} = (\sqrt{\mathcal{H}_{11}} - \sqrt{\mathcal{H}_{22}})(\sqrt{\mathcal{H}_{33}} - \sqrt{\mathcal{H}_{22}})$. If the nanotubes interact with the fiber through the solvent, in this case ethanol, the Hamaker constant results in $\mathcal{H}_{123} = 1.47 \times 10^{-20}$ J ($\mathcal{H}$ value for ethanol is shown in Table 2, $\mathcal{H}_{11(MWCN)} = 23.8 \times 10^{-20}$ J, $\mathcal{H}_{33(fused\text{-}silica)} = 6.6 \times 10^{-20}$ J).[43,50] If they interact having a gas phase in between ($\mathcal{H}_{22} \approx 0$), the resultant Hamaker constant increases by 1 order of magnitude, that is, $\mathcal{H}_{123} = 1.25 \times 10^{-19}$J, which is a typical value for condensed phases. We therefore suggest that the gas phase formed around the nanotubes at high optical powers helps them adhere to the surface of optical fibers.

DOI: 10.1021/acs.langmuir.5b02448
Langmuir 2015, 31, 10066−10075

CONCLUSIONS

In this paper. we have analyzed the motion of multiwalled carbon nanotube (MWCN) dispersions made with water or ethanol upon laser irradiation with an optical fiber. It was observed that motion occurs either inside or outside the laser beam cone, that is, motion is generated by direct momentum transfer from the electromagnetic radiation and also by thermal gradients. Fast motion movies of the dispersions revealed that MWCN clusters migrate toward the laser beam axis (hotter regions) at a maximum rate of 1 μm/s, and motion occurs faster in ethanol than in water (by a factor of 1.8−2.6).

Motivated by some theoretical works,[10,13,17,18] we adopted a simple explanation for noncharged particle thermophoretic motion in order to obtain a suitable theoretical formulation for the motion observed in this study. We proposed that thermophoresis can be described in the following terms: when a liquid is exposed to a temperature distribution, a gradient of the specific volume of the liquid (ν_o) is established due to a thermal expansion coefficient α_ν. Particle thermophoresis is therefore a thermodynamic consequence of having such ν_o gradients: they will migrate to hotter regions if particle−solvent interactions are repulsive in order to minimize the interactions per unit area (regions where ν_o attains a maximum value); on the other hand, particles will migrate to colder regions if the interactions are attractive in nature in order to maximize such interactions per unit area (regions where ν_o is a minimum). Thermal expansion of the liquid is therefore the main driving mechanism in these kinds of systems; on the other hand, it is the interaction potential between the particle and solvent that defines the thermophoretic direction. Using a repulsive potential (hydrophobic interaction) between the MWCN and the solvents, we obtained a thermophoretic velocity equation that can give the correct magnitude, and direction, of the negative thermophoretic motion observed in the experiments. The Brenner−Bielenberg formula[17] also gives the correct magnitude of the velocity but the incorrect motion direction. The formulation of Würger,[11] which conceive thermophoresis as a micro- nanoscaled version of thermocapillary flows, also gives the right magnitude and direction for the experimental velocities provided that the characteristic length r_o scales with the microstructure of the MWCN clusters ($O(1)$ nm) rather than with the whole cluster size ($O(1)$ μm). The reason why we have adopted the thermal expansion mechanism rather than the surface tension gradient effects is because the latter predicts a higher velocity in water than in ethanol (by a factor of $\sigma_{T,water}/\sigma_{T,et} \approx 1.7$), contrary to what is seen in the experiments. The thermal expansion driven mechanisms predicts, on the other hand a velocity ratio of $(\alpha_{v,water}/\nu_{o,water})/(\alpha_{v,et}/\nu_{o,et}) \approx 0.9$. Notice that our assumptions support the idea that negative thermophoresis is driven by hydrophobic interactions, which is closely connected to the concept of hydration entropy.[14] Iacopini et al.[40] have provided experimental data that actually suggest that the hydrophobic condition is not strictly necessary in order to obtain negative Soret coefficients. Hence, there is still some debate whether such negative values depend exclusively on the value of the hydration entropy, or there are still other effects that have yet to be found.

We also estimated the effects of other driving forces on the motion of the MWCN clusters, and we found that as the optical power increases, convection currents start to compete with thermophoresis and increases the particle velocity near the optical fiber axis. On the other hand, we estimated that the contribution of optical gradient forces on the accumulation of MWCN clusters at the beam axis is negligible at least in our system where the beam is not focused not even collimated.

Regarding the motion observed inside the laser cone, we found that radiative pressure is the mechanism responsible of pushing away the MWCN clusters from the fiber tip at a rate of 1 μm/s (same order of magnitude as the thermophoretic motion). In comparison, other driving forces based on light irradiation that can generate particle motion yield much higher velocities; for instance, thermophoresis driven by an asymmetric particle heating due to light absorption (named "photophoresis" in Soong et al.[27]) gives a velocity of $O(100)$ μm/s. The photophoretic velocity of carbon nanoparticles dispersed in air can actually be of order $O(1000 - 10\,000)$ μm/s.[26]

Finally, we proposed that the formation of gas−liquid interfaces (microbubbles) at high optical powers are responsible for the deposition of carbon nanoparticles on the optical fiber surfaces, as suggested by the computation of the hamaker constant (van der Waals attractive forces) of multilayered systems.

ASSOCIATED CONTENT

Supporting Information

The Supporting Information is available free of charge on the ACS Publications website at DOI: 10.1021/acs.langmuir.5b02448.

Fast-motion video of the clusters dispersed in water (AVI)

AUTHOR INFORMATION

Corresponding Author

*E-mail: jrvelez@ifisica.uaslp.mx.

Notes

The authors declare no competing financial interest.

ACKNOWLEDGMENTS

The authors appreciate financial support from Conacyt-México under Grant 154464. R.V. specially acknowledges the financial support of Cátedras Conacyt.

REFERENCES

(1) Anderson, J. L. Colloid Transport by Interfacial Forces. *Annu. Rev. Fluid Mech.* **1989**, *21*, 61−99.

(2) Brady, J. F. Brownian motion, hydrodynamics, and the osmotic pressure. *J. Chem. Phys.* **1993**, *98*, 3335−3341.

(3) Lhuillier, D. Thermodiffusion of rigid particles in pure liquids. *Phys. A* **2011**, *390*, 1221−1233.

(4) Shiundu, P.; Liu, G.; Giddings, J. C. Separation of Particles in Nonaqueous Suspensions by Thermal Field-Flow Fractionation. *Anal. Chem.* **1995**, *67*, 2705−2713.

(5) Jiang, H.-R.; Wada, H.; Yoshinaga, N.; Sano, M. Manipulation of Colloids by a Nonequilibrium Depletion Force in a Temperature Gradient. *Phys. Rev. Lett.* **2009**, *102*, 208301.

(6) Wienken, C.; Baaske, P.; Duhr, S.; Braun, D. Thermophoretic melting curves quantify the conformation and stability of RNA and DNA. *Nucleic Acids Res.* **2011**, *39*, e52.

(7) Lei, H.; Zhang, Y.; Li, X.; Li, B. Photophoretic assembly and migration of dielectric particles and Escherichia coli in liquids using a subwavelength diameter optical fiber. *Lab Chip* **2011**, *11*, 2241−2246.

DOI: 10.1021/acs.langmuir.5b02448
Langmuir 2015, 31, 10066−10075

(8) Smith, D.; Woods, C.; Seddon, A.; Hoerber, H. Photophoretic separation of single-walled carbon nanotubes: a novel approach to selective chiral sorting. *Phys. Chem. Chem. Phys.* **2014**, *16*, 5221−5228.
(9) Parola, A.; Piazza, R. Particle thermophoresis in liquids. *Eur. Phys. J. E: Soft Matter Biol. Phys.* **2004**, *15*, 255−263.
(10) Semenov, S.; Schimpf, M. Thermophoresis of dissolved molecules and polymers: Consideration of the temperature-induced macroscopic pressure gradient. *Phys. Rev. E* **2004**, *69*, 011201.
(11) Würger, A. Thermophoresis in Colloidal Suspensions Driven by Marangoni Forces. *Phys. Rev. Lett.* **2007**, *98*, 138301.
(12) Schermer, R.; Olson, C.; Coleman, J.; Bucholtz, F. Laser-induced thermophoresis of individual particles in a viscous liquid. *Opt. Express* **2011**, *19*, 10571−10586.
(13) Piazza, R.; Parola, A. Thermophoresis in colloidal suspensions. *J. Phys.: Condens. Matter* **2008**, *20*, 153102−18.
(14) Duhr, S.; Braun, D. Why molecules move along a temperature gradient. *Proc. Natl. Acad. Sci. U. S. A.* **2006**, *103*, 19678−19682.
(15) Dhont, J. K. G.; Wiegand, S.; Duhr, S.; Braun, D. Thermodiffusion of Charged Colloids: Single-Particle Diffusion. *Langmuir* **2007**, *23*, 1674−1683.
(16) Ning, H.; Dhont, J. K. G.; Wiegand, S. Thermal-Diffusive Behavior of a Dilute Solution of Charged Colloids. *Langmuir* **2008**, *24*, 2426−2432.
(17) Brenner, H.; Bielenberg, J. R. A continuum approach to phoretic motions: Thermophoresis. *Phys. A* **2005**, *355*, 251−273.
(18) Semenov, S.; Schimpf, M. Statistical Thermodynamics of Material Transport in Nonisothermal Suspensions. *J. Phys. Chem. B* **2015**, *119*, 3510−3516.
(19) Würger, A. Heat capacity-driven inverse Soret effect of colloidal nanoparticles. *Europhys. Lett.* **2006**, *74*, 658−664.
(20) Plyukhin, A. Thermophoresis as persistent random walk. *Phys. Lett. A* **2009**, *373*, 2122−2124.
(21) Hottovy, S.; Volpe, G.; Wehr, J. Thermophoresis of Brownian particles driven by coloured noise. *Europhys. Lett.* **2012**, *99*, 60002−6.
(22) Desyatnikov, A.; Shvedov, V.; Rode, A.; Krolikowski, W.; Kivshar, Y. Photophoretic manipulation of absorbing aerosol particles with vortex beams: theory versus experiment. *Opt. Express* **2009**, *17*, 8201−8211.
(23) Hirai, A.; Monjushiro, H.; Watarai, H. Laser Photophoresis of a Single Droplet in Oil in Water Emulsions. *Langmuir* **1996**, *12*, 5570−5575.
(24) Monjushiro, H.; Hirai, A.; Watarai, H. Size Dependence of Laser-Photophoretic Efficiency of Polystyrene Microparticles in Water. *Langmuir* **2000**, *16*, 8539−8542.
(25) Beresnev, S.; Chernyak, V.; Fomyagin, G. Photophoresis of a spherical particle in a rarefied gas. *Phys. Fluids A* **1993**, *5*, 2043−2052.
(26) Shvedov, V.; Rode, A. V.; Izdebskaya, Y. V.; Desyatnikov, A. S.; Krolikowski, W.; Kivshar, Y. S. Giant Optical Manipulation. *Phys. Rev. Lett.* **2010**, *105*, 118103.
(27) Soong, C. Y.; Li, W. K.; Liu, C. H.; Tzeng, P. Y. Theoretical analysis for photophoresis of a microscale hydrophobic particle in liquids. *Opt. Express* **2010**, *18*, 2168−2182.
(28) Ham, H. T.; Choi, Y. S.; Chung, I. J. An explanation of dispersion states of single-walled carbon nanotubes in solvents and aqueous surfactant solutions using solubility parameters. *J. Colloid Interface Sci.* **2005**, *286*, 216−223.
(29) Huang, Y. Y.; Terentjev, E. M. Dispersion of Carbon Nanotubes: Mixing, Sonication, Stabilization, and Composite Properties. *Polymers* **2012**, *4*, 275−295.
(30) Tan, S.; Lopez, H. A.; Cai, C. W.; Zhang, Y. Optical Trapping of Single-Walled Carbon Nanotubes. *Nano Lett.* **2004**, *4*, 1415−1419.
(31) Xin, H.; Li, X.; Li, B. Massive photothermal trapping and migration of particles by a tapered optical fiber. *Opt. Express* **2011**, *19*, 17065−17074.
(32) Hartschuh, A.; Pedrosa, H. N.; Peterson, J.; Huang, L.; Anger, P.; Qian, H.; Meixner, A. J.; Steiner, M.; Novotny, L.; Krauss, T. D. Single Carbon Nanotube Optical Spectroscopy. *ChemPhysChem* **2005**, *6*, 577−582.
(33) Plewa, J.; Tanner, E.; Mueth, D. M.; Grier, D. G. Processing carbon nanotubes with holographic optical tweezers. *Opt. Express* **2004**, *12*, 1978−1981.
(34) Rusconi, R.; Isa, L.; Piazza, R. Thermal-lensing measurement of particle thermophoresis in aqueous dispersions. *J. Opt. Soc. Am. B* **2004**, *21*, 605−616.
(35) Brothers, E.; Izmaylov, A.; Scuseria, G.; Kudin, K. Analytically calculated polarizability of carbon nanotubes: single wall, coaxial, and bundled systems. *J. Phys. Chem. C* **2008**, *112*, 1396−1400.
(36) Walther, J.; Jaffe, R.; Halicioglu, T.; Koumoutsakos, P. Carbon Nanotubes in Water: Structural Characteristics and Energetics. *J. Phys. Chem. B* **2001**, *105*, 9980−9987.
(37) Werder, T.; Walther, J. H.; Koumoutsakos, P. Hydrodynamics of Carbon Nanotubes - Contact Angle and Hydrophobic Hydration. *Tech. Proc. 2002 Int. Conf. Comput. Nanosci. Nanotechnol.* **2002**, *2*, 490−493.
(38) Kedenburg, S.; Vieweg, M.; Gissibl, T.; Giessen, H. Linear refractive index and absorption measurements of nonlinear optical liquids in the visible and near-infrared spectral region. *Opt. Mater. Express* **2012**, *2*, 1588−1611.
(39) Sammarco, T. S.; Burns, M. A. Thermocapillary Pumping of Discrete Drops in Microfabricated Analysis Devices. *AIChE J.* **1999**, *45*, 350−366.
(40) Iacopini, S.; Rusconi, R.; Piazza, R. The "macromolecular tourist": Universal temperature dependence of thermal diffusion in aqueous colloidal suspensions. *Eur. Phys. J. E: Soft Matter Biol. Phys.* **2006**, *19*, 59−67.
(41) Derjaguin, B. V.; Churaev, N. V.; Muller, V. M. *Surface Forces*; Consultants Bureau (Plenum): New York, 1987.
(42) Morthomas, J.; Würger, A. Thermophoresis at a charged surface: the role of hydrodynamic slip. *J. Phys.: Condens. Matter* **2009**, *21*, 035103−4.
(43) Israelachvili, J. *Intermolecular and Surface Forces*; Elsevier: Amsterdam, 2011.
(44) Shvedov, V. G.; Desyatnikov, A. S.; Rode, A. V.; Krolikowski, W.; Kivshar, Y. S. Optical guiding of absorbing nanoclusters in air. *Opt. Express* **2009**, *17*, 5743−5757.
(45) Morozov, K. I.; Köhler, W. Thermophoresis of Polymers: Nondraining vs Draining Coil. *Langmuir* **2014**, *30*, 6571−6576.
(46) Taylor, R. S.; Hnatovsky, C. Trapping and mixing of particles in water using a microbubble attached to an NSOM fiber probe. *Opt. Express* **2004**, *12*, 916−928.
(47) Kashiwagi, K.; Yamashita, S.; Set, S. Y. Optically formed carbon nanotube sphere. *Opt. Express* **2008**, *16*, 2528−2532.
(48) Zheng, Y.; Liu, H.; Wang, Y.; Zhu, C.; Wang, S.; Cao, J.; Zhu, S. Accumulating microparticles and direct-writing micropatterns using a continuous-wave laser-induced vapor bubble. *Lab Chip* **2011**, *11*, 3816−3820.
(49) Pimentel-Dominguez, R.; Hernández-Cordero, J.; Zenit, R. Microbubble generation using fiber optic tips coated with nanoparticles. *Opt. Express* **2012**, *20*, 8732−8740.
(50) Domínguez, H. Structure of the SDS/1-dodecanol surfactant mixture on a graphite surface: A computer simulation study. *J. Colloid Interface Sci.* **2010**, *345*, 293−301.

DOI: 10.1021/acs.langmuir.5b02448
Langmuir 2015, 31, 10066−10075